


# NSTTF Heliocon Wireless Closed-Loop Controls Test Bed Development

Kenneth Armijo<sup>1</sup>, Haden Harper<sup>1</sup>, Zachary Bernius<sup>1</sup>, Claus Danielson<sup>2</sup>, Ansel Blumenthal<sup>1</sup> and Luis Garcia-Maldonado<sup>1</sup>

<sup>1</sup> Concentrating Solar Technology, Sandia National Laboratories, Albuquerque, NM, USA

<sup>2</sup> University of New Mexico, Albuquerque, NM, USA

\*Correspondence: Kenneth Armijo, [kmarmij@sandia.gov](mailto:kmarmij@sandia.gov)

**Abstract.** A closed loop controls test bed is in development at the Sandia National Laboratories (SNL), National Solar Thermal Test Facility (NSTTF) as part of the U.S. DOE SETO sponsored Heliostat Consortium (HeliOCON) program. This work pertains to preliminary development of advanced feedback controls for a concentrating solar power (CSP) field of 218 heliostats, and the development of a baseline closed-loop controls extremum seeking control (ESC) algorithm. This algorithm utilizes a batch least squares (BLS) technique to facilitate feedback control automation for heliostat pointing. This allows the determination of the optimal highest flux within a Gaussian profile, for both a four-point (QuadCell) aim point strategy, and a concentric aim point strategy. The results of this work determined that both approaches using the ESC BLS were able to reduce pointing errors to zero for both azimuth and elevation heliostat position movements. This work also reviews progress of the test bed which will allow flexible employment of controls and sensors which will be communicating with both wired and wireless protocols. The solar field distributed control system (DCS) will manage the flux distribution of energy across test articles and solar receivers using real-time programmable logic controllers (PLC) at each heliostat, for aiming and closed-loop feedback. Feedback control will be facilitated with a variety of sensors, located: 1. On the heliostat, 2. On the tower or 3. At an ancillary field tower station. The system is also developed to incorporate environmental information to provide real-time feedback into advanced algorithms for solar field management.

**Keywords:** Heliostat Field, Closed Loop Controls, Test Bed, Wireless Communications

## 1. Heliostat Closed Loop Controls

### 1.1 Overview

Reduction in communication and controls equipment through wireless architectures can reduce the need for cabling by as high as 42%, which can significantly drive down overall deployment costs, compared to a fully wired system, representative of the state-of-the-art technology for commercial power tower plants” [1]. Research by Pfahl characterized tracking accuracy from outside influences including deviations that can arise from backlash in tandem with high wind loads, as well as systematic errors. It was described that closed loop controls systems are only limited by range of motion, measurement accuracy of a feedback sensor, and motor control. Difficult influences like deformation under gravity, wind and temperature can be compensated as long as the sensor-heliostat calibration stays intact. Tracking accuracy

can be improved in closed loop systems with high fidelity cameras and pointing sensors, which can reduce spillage and allow better control of heliostat fields to achieve a certain overall flux distribution [2]. However, closed loop controls can vary greatly across different commercial architectural platforms and fields [3]. The SNL NSTTF is therefore developing a novel wireless, closed-loop controls flexible test bed to assess different closed-loop controls and wireless communications approaches to de-risk commercial deployments.

## 1.2 Baseline Closed Loop Controls Design

In this investigation a closed loop controller was developed to manipulate heliostat clusters to produce maximum reflectance onto a receiver to produce the highest possible power output, as shown in Figure 1. Here, the controller adjusts the angle of the heliostat to maximize power received. Traditionally, an open-loop GPS timer is used to send tracking signals to heliostat mirrors to achieve general positioning on a receiver, however tracking and pointing errors can accrue over time [4]. To reduce these errors a closed loop Extremum Seeking Control algorithm (ESC) was developed with gradient ascent to find the azimuth and elevation angle to adjust individual heliostats to a maximum flux profile. A challenge in the development of this algorithm is not having a prior known power function to calculate the true gradient. Even if there is a known power function, the function would not take into account unknown variables that could have a negative effect on power received such as wind. There could also be time-varying disturbances that could have negative effects on the power, meaning an estimated gradient must be used. To estimate the gradient, a batch least squares algorithm (BLS) was utilized, with power measurements obtained at different azimuth and elevation angle positions.

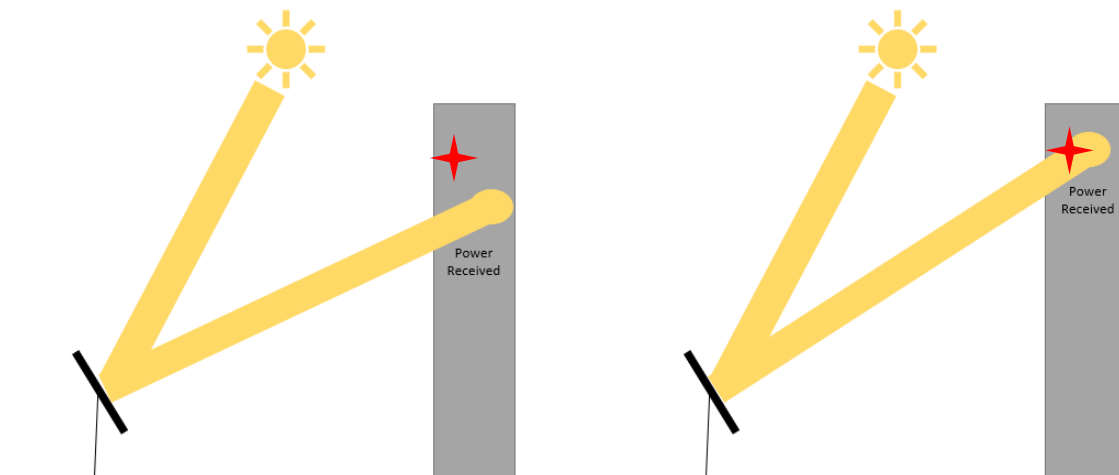


**Figure 1.** Diagram of Heliostat Concentrating Sun on the Receiver. Left figure shows initial non-optimal pointing. Right figure is after the controller has adjusted heliostats to provide maximum power received.

The closed loop controller presented here consists of two different stages. The first is a feedforward controller, which is an open loop control algorithm that uses the time of day and year to get obtain an initial azimuth and elevation. The second stage will be a feedback controller that uses ESC and BLS to give fine-tuned adjustments to maximize receiver power. This paper will focus on the feedback controller. This approach assumes later stage power sensors would be placed on the tower for controls measurement feedback and communication with respect to heliostat motor encoder motion control. Figure 2 shows the structure of the feedback loop. The heliostat input will be a desired azimuth and elevation angle,  $r(t)$ , and the heliostat dynamics are modeled by the transfer function,  $H(s)$ . Once the heliostats move, the encoders will give an actual azimuth and elevation angle,  $y(t)$ , which requires some finite-time to converge to the desired set-point,  $r(t)$ . The power distribution,  $P(y)$ , will then be measured from our sensors on the tower. The values of  $r(t)$  and  $y(t)$  are known. This is a feed-back loop, requiring control-theoretic analysis to ensure stability. Extremum seeking control is a real-time

data-driven optimization algorithm that finds the optimal azimuth and elevation angle ( $r^*$ ) where the maximum power ( $P^*$ ) is received on the tower. The power function is concave and therefore maximized if and only if the gradient at the location is equal to 0 ( $\nabla P = 0$ ). The goal of the ESC algorithm is to drive the gradient to zero ( $\nabla P \rightarrow 0$ ). To find the optimal azimuth and elevation, an estimated non-zero gradient ( $\nabla P$ ) is used to find a direction that increases power, using the steepest ascent optimization algorithm:

$$r^+ = r + K\nabla P \quad (1)$$

The controller portion of the feedback loop will add the gradient, multiplied by some gain ( $K$ ), to the current location of the heliostat. This new azimuth and elevation will be inputted to the integrator, the controller that communicates to the heliostat, to move our heliostat. Following the gradient to the new location ( $r^+$ ) increases the power received:  $P(r + K\nabla P) > P(r)$ . Then the process repeats with a re-calculation of the gradient estimate at the new position to improve the power and move the heliostat.

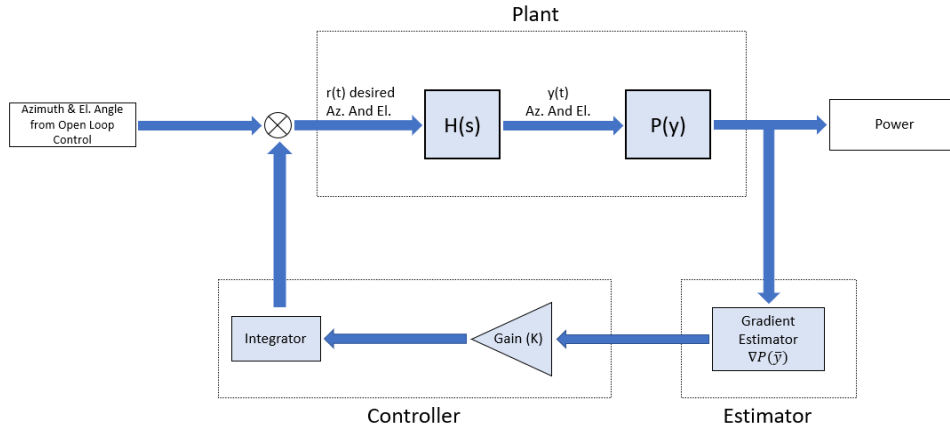


**Figure 2.** ESC Block Diagram. The Plant contains the dynamics for the heliostat as a transfer function  $H(s)$  and the measured values of  $P(y)$ .

The ESC algorithm uses data to estimate the gradient for a power measured at a particular location,  $P_i = P(y_i)$ , where  $y_i$  is the azimuth and elevation angle. The estimator portion of the loop uses the BLS algorithm to estimate the gradient. A measured Power versus Position inputted into the estimator using real-time dataset to provide us with feedback.

$$\{P_i, y_i\}_{i=1}^N \quad (2)$$

To estimate the gradient, we begin with our initial power function, where the measured power is taken at some proposed improved direction. In this problem formulation, all the values are known except the value of  $\nabla P(\bar{y})$ , the estimated gradient at  $\bar{y}$ ; the Least-Squares Estimator is then implemented. To minimize the estimation error of the Estimator, a derivative is taken with the goal to find when the derivative of  $E$  is equal to 0. To derive the BLS algorithm  $\theta = (\Phi\Phi^T)^{-1}\Phi P_i$ , an approximation is found of the unknown power function by a first-order Taylor-series, where the values of  $P_i$  and  $y_i$  are measured and the values of  $P(\bar{y})$  and  $\nabla P(\bar{y})^T$  are estimated. The estimated values appear linearly in the Taylor-series, which allows the use of BLS instead of another algorithm.

$$P_i \approx P(\bar{y}) + \nabla P(\bar{y})^T (y_i - \bar{y}) = \theta^T \Phi_i \quad (3)$$

$$\Phi_i = \begin{bmatrix} 1 \\ y_i - \bar{y} \end{bmatrix}$$

$$\theta = \begin{bmatrix} P(\bar{y}) \\ \nabla P(\bar{y}) \end{bmatrix}$$

Using the Taylor approximation (Eqn. 4), an estimation error can be defined where  $P_i - \theta^T \Phi$  is the error produced by the estimate,  $\theta$ , for the  $i$ th data point. The Least-Squares Estimator,  $E$ , chooses the estimate,  $\theta$ , that minimizes the squared estimation errors. To minimize the cost of the Estimator, a derivative is taken with the goal of finding when the derivative of  $E$  is equal to 0.

$$E = \frac{1}{2}(P_i - \theta^T \Phi)^2 \quad (4)$$

Since the estimation problem is unconstrained and convex, the optimal estimate,  $\theta^*$ , can be obtained by setting the derivative to zero, where the vector  $\frac{dE}{d\theta}$ , contains derivatives of the squared estimation error with respect to  $P(\bar{y})$  and  $\nabla P(\bar{y})$ . Taking the derivative of the estimator with respect to  $\theta$  and setting it equal to 0, we can solve for  $\theta$ . The estimated gradient can be pulled out of the  $\theta$  matrix to use in the controller discussed above.

$$\frac{dE}{d\theta} = \Phi P_i - \Phi \Phi^T \theta = 0 \quad (5)$$

$$\theta = (\Phi \Phi^T)^{-1} \Phi P_i \quad (6)$$

An advantage of this formulation is that the algorithm can calculate the estimated gradient when a dataset is sufficient. For the dataset to be sufficient, it must be persistently exciting, meaning that the data needs to be unique. The algorithm needs persistently exciting data to make  $(\Phi \Phi^T)$  invertible. The BLS estimator becomes more effective as the excitation of the data increases.

### 1.3 Estimator Discussion & Results

To validate the ESC algorithm, simulations have been designed to compare the estimated gradient to the actual gradient of a known power function. The goal of the ESC algorithm is to find peak power at the center of the receiver. We are assuming that the power function on the solar tower can be approximated by a Gaussian profile. We began by using Eqn. 7 for a 2-variable Gaussian profile,

$$f(x_1, \dots, x_k) = \frac{\exp(-\frac{1}{2}(x-\mu)^T \Sigma^{-1}(x-\mu))}{\sqrt{2\pi^k |\Sigma|}} \quad (7)$$

where  $\mu$  and  $\Sigma$  are the mean vector and covariance matrix, respectively, to develop a power function for our simulations. With this known equation, we can analytically compute the derivative to find what the true gradient is at each point. This calculated gradient was used to validate the estimated gradient from the BLS. A grid mesh is built to act as our power function as shown below in Fig. 3. In the three simulations, a comparison was made of the BLS estimated gradient to the true gradient at each point.

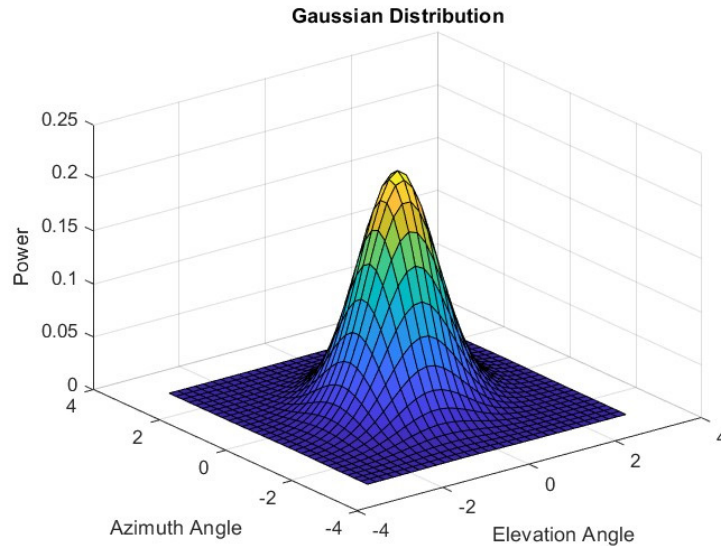


**Figure 3.** Gaussian Power Function. The figure shows the ESC power distribution across each azimuth and elevation angle.

For the first simulation, four heat flux sensors were used in a configuration as shown in Fig. 4 below, to determine the peak power. The goal of this simulation was to compare this data collection method and estimation with the true gradient at each point. When the box is at the center of the solar beam, the power at each point will be the same, meaning the gradient is zero across the four sensors. In each simulation, estimations of the gradient are made at each point in the mesh. The vectors for the estimated gradient are scaled down for clarity.

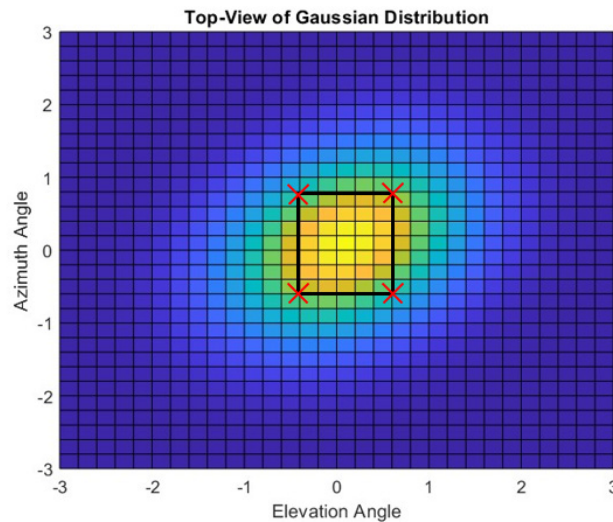


**Figure 4.** QuadCell Heatflux Gauge Simulation Concept. The figure shows the location of the QuadCell sensors (red x's) and the power distribution.

The Quadcell simulation results are shown in Fig. 5. Note that that the estimated gradient and the calculated gradient are very similar. The estimated gradient goes in the same direction as the calculated gradient. As the algorithm gets closer to the optimal value, the error between the calculated and estimated gradient go to zero. The calculated and estimated gradient each point towards peak power, meaning the estimator accomplishes the goal of finding the optimal azimuth and elevation. This validates the gradient estimator because it shows data points around a given position can be used to find an accurate estimation of the gradient. From this we also wanted to know the error between the estimated and calculated gradient with the zero

error as we approach the optimal target. This validates BLS estimator to give an accurate location for optimal azimuth and elevation.

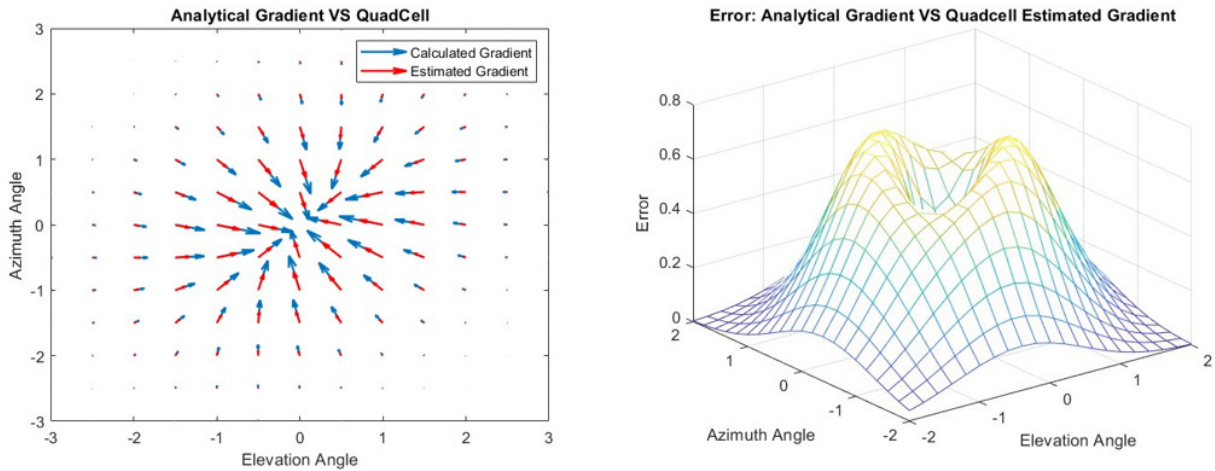


**Figure 5.** QuadCell Simulation Results. Left figure shows calculated versus estimated gradient from algorithm using QuadCell configuration. Right figure is the error between the calculated gradient and estimated gradient.

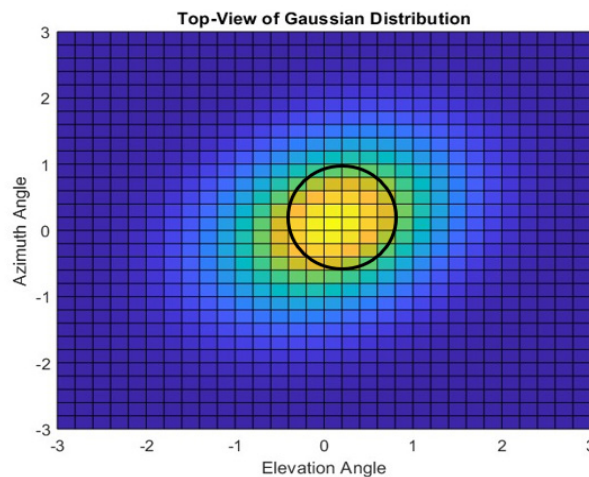


**Figure 6.** Concentric Heatflux Gauge Simulation Concept. Figure shows location of the sensor (black circle) and power distribution. Optimal location is the center of the sensor and peak power.

For the next simulation, a concentric heat flux gauge was used to measure heat flux on the entirety of the circumference of the circle shown in Fig. 6. The concentric heat flux gauge results are shown in Fig. 7. It is shown that the estimated gradient goes in the same direction as the calculated gradient. The error between the calculated gradient and estimated gradient, for the concentric heatflux gauge also approaches zero as the algorithm approaches the optimal azimuth and elevation. This parallels the results from the Quadcell simulation and further validates the estimator because the estimated gradient is consistently accurate through different data collection methods.

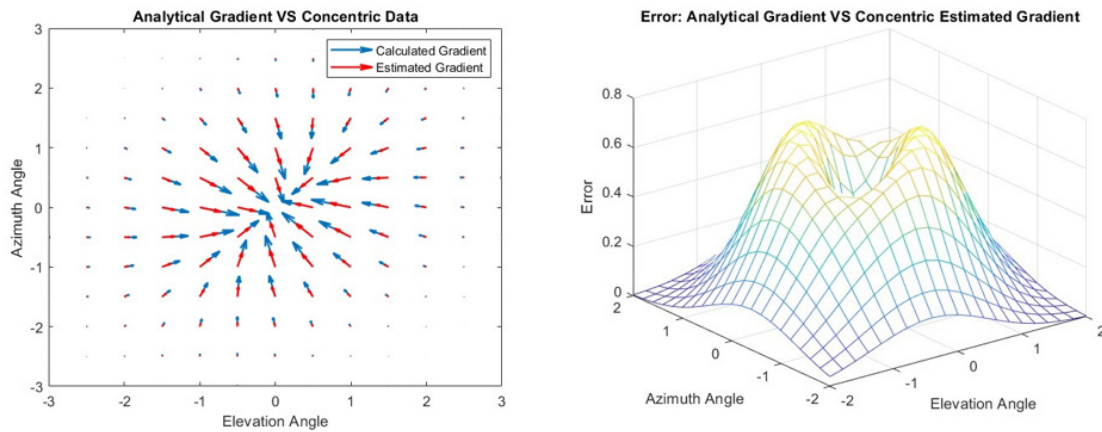


**Figure 7.** Concentric Heat Flux Gauge Simulation Results. Left figure is calculated versus estimated gradient using Concentric Heat Flux Gauge configuration. Right figure is calculated and estimated gradient error.

The estimated gradient provided similar results to the calculated gradient. The significance of this is confidence using the gradient ascent algorithm to move the heliostat towards the optimal azimuth and elevation at a gradient equal to zero.

### 1.4 ESC Discussion/Results

In this next simulation, pixel data is taken from a camera; 2,601 pixels can be used as data points for this simulation to show that the algorithm climbs the gradient until we reach the optimal azimuth and elevation. In the simulation, a starting pixel coordinate of (30,20) is used with the optimal azimuth and elevation located at a pixel coordinate of (26,26). The MATLAB code will iterate and climb the gradient until we converge to a gradient of zero at the optimal pixel of (26,26).

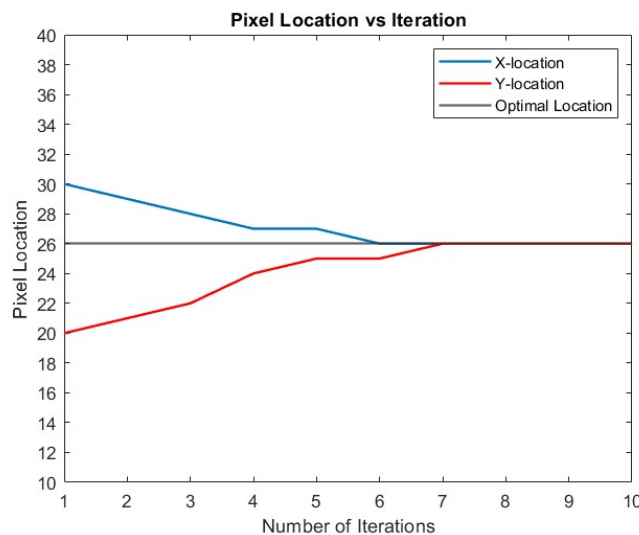


**Figure 8.** Optimal Convergence Simulation Results. The figure shows the pixel location after each iteration. The pixel location converges to the optimal pixel location.

In Figure 8, we can see the algorithm reaching the optimal azimuth and elevation, pixel (26,26), around 7 iterations. This figure shows that we are in fact ascending the gradient to the maximum of our theoretical power function. This is significant because it allows the algorithm to converge at a very low iteration which would allow the controller to send a new azimuth and elevation to the heliostat within a few seconds which allows accurate tracking as the sun is moving throughout the sky. When using this on a heliostat, the sun will be tracked as it moves

and will be chasing the optimal azimuth and elevation of a dynamic system. In this simulation we are not tracking a dynamic system, we are just ascending a static power function. These simulations give us confidence the algorithm will perform as expected on a heliostat.

There are many challenges involved with ESC design. One challenge is that the feedback-loop can go unstable if our initial point is too far from the optimal and/or our gain is too large. Other challenges include parts of the feedback-loop being unknown, such as the power function and the use of data-driven methods to learn, which involves noise from measurements. Despite these challenges, the algorithm developed will converge to an optimal location quickly and accurately.

## 2. Wireless Communications Test Bed Development

This work also includes the development of a flexible wireless communications overlaid test bed on top of the developed controls within section 1. Initially the team considered varying communication strategies for single as well as groups of heliostats, with a single power tower, or intermediate communication towers. Closed loop controls communications require confident signal transmission and processing speeds from heliostat controllers and field control sensors. These can be used to determine optimal positions for each respective heliostat, accounting for environmental conditions and receiver flux mapping conditions of a project site [5]. For example, the SFINCS control system [6] manages the distribution of energy across the solar receiver using real-time heliostat-aiming and closed-loop feedback algorithms for solar field. On-site weather systems, and visual and infrared cameras provide real-time feedback into advanced algorithms for solar field management. Proprietary optimization and control software maximizes project performance and power production efficiencies" [7]. From this information, it can be deduced that proprietary heliostat aiming occurs in tandem with infrared cameras directed at the target to send feedback through a comms network to a control tower with data of flux density resolution.

A reduction in materials using wireless communications is especially promising. Initial research completed by HeliCon has found for wireless heliostat fields "The need for electrical cabling is thereby reduced by 85% or more" [8]. Materials saved through this employment can significantly lower costs of a shared-node wireless system to be 42% less than the cost of a fully wired system for traditional commercial power tower plants" [8]. Pfahl previously discussed tracking accuracy from outside influences including deviations that can arise from backlash in tandem with high wind loads, as well as systematic errors. The research found that closed loop control systems can be primarily limited by dynamic motions, measurement accuracy of the feedback sensor, and motor control [9]. Difficult influences like deformation under gravity, wind and temperature can be compensated as long as the sensor-heliostat calibration stays intact. Tracking accuracy can however be better in closed loop systems which can reduce spillage and allow better control of the whole field of heliostats to achieve a certain overall flux distribution [9]. This affirms the need for highly accurate wireless controls. For the NSTTF heliostats, the team is installing a wireless transmitter which would provide baseline Wifi communications up to 100 Mbp, as well as five Wireless Network Switches (WNS, which would act as communication receivers). The overall system would also require a Wireless Network Bridge (WNB) antenna in the field as well as an Ubiquiti Air Fiber Wireless Bridge (AFWB) antenna within the control room. Having individual transmitters for each heliostat will create a network of nodes for a strong signal. In parallel the team is also installing a wireless mesh network that can operate on wireless communication protocols. These assessed wireless systems, will be compared to each other to investigate varying mesh network and wifi protocols, as well as signal congestion, intermittenencies and loss of signal (LOS) issues. The test bed includes installation of a wireless Wifi transmitter at each heliostat with communication rates up to 100 Mbp, as well as five Wireless Network Switches (WNS, which would act as communication receivers). Wireless latency is being characterized for varying heliostat field operational configurations and modes, as well as scalability to add additional heliostats, which



may cause potential bandwidth challenges for a growing field. This test bed will be used to explore cyber security challenges to allow controlled attempts at disrupting communication signals between the heliostats and the control tower. These will be facilitated based simulations through SPICE and Python software. The system also includes a parallel mesh network system where a wireless Radio Frequency (RF) transmitter will be installed and tested for each respective heliostat. The wireless communication system is developed from the commercially available SmartMesh IP technology. A past Solar Dynamics project successfully demonstrated this technology's capabilities in a limited solar field-testing campaign [10]. This technology is also being applied and compared to the wifi network with respect to communication and optical metrology metrics, such as signal congestion, pointing error and off-axis tracking. The architecture for the test bed is presented in Figure 9, between the control room digital signal controller (DSC) computer, and each heliostat's PLC. All 218 controllers are configurable for the single DSC or operated independently via local manual control.

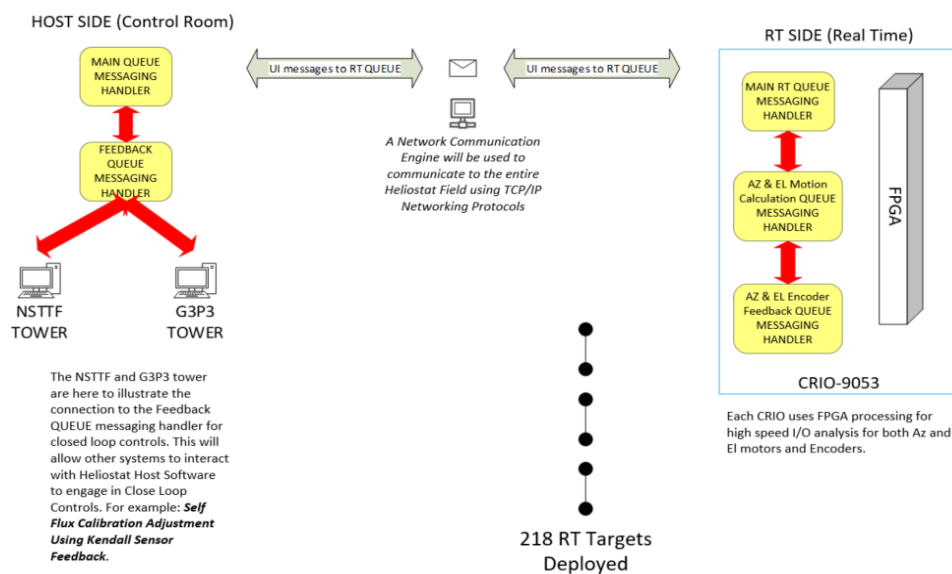


Figure 9. SNL NSTTF Heliostat Field Wireless Closed Loop Controls Communications Design.

This closed loop controls test bed is being developed with respect to heliostat controls feedback communication with a new DOE Generation 3 Pilot Plant (G3P3) system. The heliostat controls will include pointing and focusing operations with respect to the thermodynamic process data acquisition at each of the various levels of the new test tower. These same feedback tower controls will also be made available to the current solar tower that has four primary areas for facilitating CSP receiver and thermodynamic systems evaluation.

### 3. Conclusions

A novel, wireless closed loop controls test bed is being developed and presented here for incorporating heliostat field industry feedback sensors technology and wireless communications to a field-wide level via the NI cRIO 9053 chassis with modern FPGA capabilities. The NSTTF Testbed will serve as a large-scale testing facility with 218 heliostats available for collaborators to investigate interoperability of controls between the heliostat field and the environment, experimentation with the use of closed loop control technology, and performance tests for comparative results between wired and wireless controls. The technical requirements of the wireless closed loop controls testbed at the NSTTF will be parceled into Operational Procedures and Implementation Plan that will be presented. Two extremum seeking closed-loop controls architectures were derived for Quadcell gradient and concentric estimated gradient approaches. Both models were able to predict movement towards zero-

error peak values. Further work is on-going to validate these approaches through experimentation at SNL for reliable pointing accuracy.

## Data availability statement

The data for this research work can be accessed directly from the authors.

## Underlying and related material

Related materials can be obtained directly from the authors.

## Competing interests

The authors declare no competing interests.

## Acknowledgements

Sandia National Laboratories is a multimission laboratory managed and operated by National Technology and Engineering Solutions of Sandia, LLC., a wholly owned subsidiary of Honeywell International, Inc., for the U.S. Department of Energy's National Nuclear Security Administration under contract DE-NA0003525.

## References

- [1] Zhu, G., Augustine, C., Mitchell, R., Muller, M., Kurup, P., Zolan, A., Yellapantula, S., Brost, R., Armijo, K., Sment, J. and Schaller, R., 2022, NREL/TP-5700-83041, NREL, Golden, CO, USA.
- [2] Pfahl, A., Coventry, J., Röger, M., Wolfertstetter, F., Vásquez-Arango, J.F., Gross, F., Arjomandi, M., Schwarzbözl, P., Geiger, M. and Liedke, P., 2017, *Solar Energy*, 152, pp.3-37.
- [3] Sattler, J.C. et al., 2020, *Sol. Energy*, vol. 207, pp. 110–132.
- [4] Malan, K. and Gauche, P., 2014. Model based open-loop correction of heliostat tracking errors. *Energy Procedia*, 49, pp.2118-2124.
- [5] Mahboob, K., Khan, M.N., Rasool, M., Nawaz, M.Q., Awais, Q., Fawad, T. and Khan, A., 2019. Control system selection for heliostat of concentrated solar thermal tower power plant. *Pakistan Journal of Science*, 71(4), p.150.
- [6] Grange, B. and Flamant, G., 2021. Aiming strategy on a prototype-scale solar receiver: Coupling of tabu search, ray-tracing and thermal models. *Sustainability*, 13(7), p.3920.
- [7] Bobinecz, M., 2012, September. Ivanpah solar electric generating facility. In *Proceedings of Engineering and construction contracting conference*.
- [8] Zhu, G., Augustine, C., Mitchell, R., Muller, M., Kurup, P., Zolan, A., Yellapantula, S., Brost, R., Armijo, K., Sment, J. and Schaller, R., 2022. Roadmap to Advance Heliostat Technologies for Concentrating Solar-Thermal Power (No. NREL/TP-5700-83041). National Renewable Energy Lab. (NREL), Golden, CO (United States).
- [9] Pfahl, A., Coventry, J., Röger, M., Wolfertstetter, F., Vásquez-Arango, J.F., Gross, F., Arjomandi, M., Schwarzbözl, P., Geiger, M. and Liedke, P., 2017. Progress in heliostat development. *Solar Energy*, 152, pp.3-37.
- [10] Kurup, P., Akar, S., Glynn, S., Augustine, C. and Davenport, P., 2022, NREL/TP-7A40-80482, NREL, Golden, CO, USA.